Measurements of the Effects of Gravity Waves in the Middle Atmosphere Using Parametric Models of Density Fluctuations. Part II: Energy Dissipation and Eddy Diffusion

R. J. SICA

Department of Physics and Astronomy, University of Western Ontario, London, Ontario, Canada

(Manuscript received 12 July 1996, in final form 17 June 1998)

ABSTRACT

Part I of this series demonstrated the advantages of parametric models in estimating the gravity wave spectrum from density fluctuation measurements using a large power-aperture-product Rayleigh-scatter lidar. The spectra calculated using the parametric models are now used to estimate energy dissipation due to gravity waves. Energy dissipation for an individual wave in the spectrum is also estimated using Prony's method, which allows the frequency, amplitude, damping, and phase of individual waves to be estimated. These two independent estimates of energy dissipation highlight the variability of the energy dissipation on short timescales due to gravity waves and turbulence. A combination of the information obtained from the parametric models of the spatial and temporal spectra with the theoretical work of M. E. McIntyre is used to estimate profiles of the eddy diffusion coefficient. This estimate attempts to include the degree of saturation of the vertical wavenumber spectrum, which determines the constant used in the calculation of the eddy diffusion coefficient. The height profile of the eddy diffusion coefficient thus obtained in the upper stratosphere and mesosphere is in good agreement with previous estimates. The degree of saturation of the vertical wavenumber spectrum is shown to increase proportionally to the Hines parameter, a measure of the transition wavenumber from a linear to a nonlinear tail spectrum. It is speculated that this fact can be interpreted as a change in the atmosphere from an ''amplifier'' state where the tail spectrum is highly nonlinear, but weak when the spectral ''gain'' is high, to a state of saturation where the high wavenumber tail spectrum is more linear, but has lower gain and more energy available to dissipate at smaller spatial scales.

1. Introduction

In Part I of this study Sica and Russell (1999, henceforth SR) present vertical wavenumber and temporal spectra in the upper stratosphere and mesosphere for the night of 30 August 1994 that highlight the intermittency of gravity wave activity in the middle atmosphere. It is also shown in SR that the kinetic energy density, on the whole, tends to decrease with altitude. Thus, it is reasonable to expect that some energy from the gravity wave sources in the lower atmosphere is being dissipated in the upper stratosphere and mesosphere as the waves propagate through the these regions.

Quantitative measurements of the dissipation of wave energy are important for general circulation models of the middle atmosphere, which may require knowledge of the gravity wave energy dissipation for realistic calculations of temperature and wind. However, a paucity of measurements of the relevant eddy diffusion coefficient exist in the upper stratosphere and mesosphere to help guide the choice of this parameter for the model calculations.

Energy dissipation and eddy diffusion have been measured by a number of different techniques in the boundary layer and near the mesopause (Hocking 1991). In the upper stratosphere and lower mesosphere it is difficult to make radar measurements of turbulence, particularly at night. The altitude range is too high for balloonborne in situ measurements but can be accessed for short periods of time at high spatial resolution by rocket payloads (e.g., Blix et al. 1990). In this paper two independent techniques are used to find the energy dissipation due to gravity waves, one a spectral technique and the other tracking individual waves. This energy dissipation is then converted into an eddy diffusion coefficient, which includes an estimate of the vertical wavenumber spectrum's saturation.

2. The measurements

The data series and spectrum used for this study are the same as detailed in SR. The measurements are from an approximately 6-h period on 30 August 1994. The measurements commenced at 0319 UTC (2319 EDT). The density fluctuation measurements were made with

Corresponding author address: Dr. Robert J. Sica, Department of Physics and Astronomy, University of Western Ontario, London, ON N6A 3K7 Canada.
E-mail: sica@uwo.ca

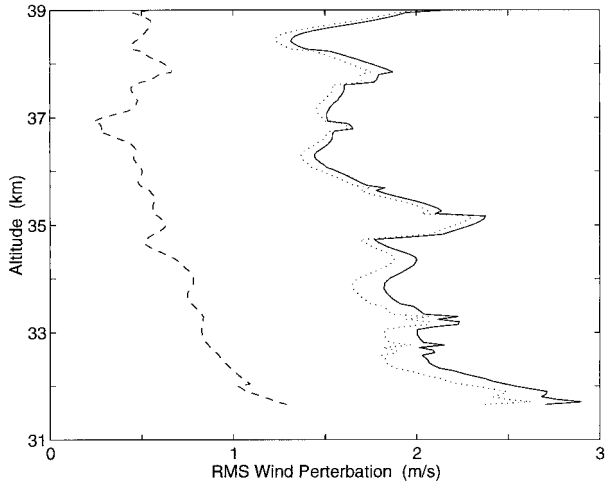

FIG. 1. Rms wind speed determined by the spectral method for three different integration limits. The solid curve and dotted curve have lower integration limits of the sampling period 1/(6 h). The solid curve has an upper integration limit of the Nyquist frequency 1/(121 s) and the dotted curve the buoyancy frequency 1/(294 s). The dashed curve has a lower integration limit of the buoyancy frequency and an upper integration limit of the Nyquist frequency.

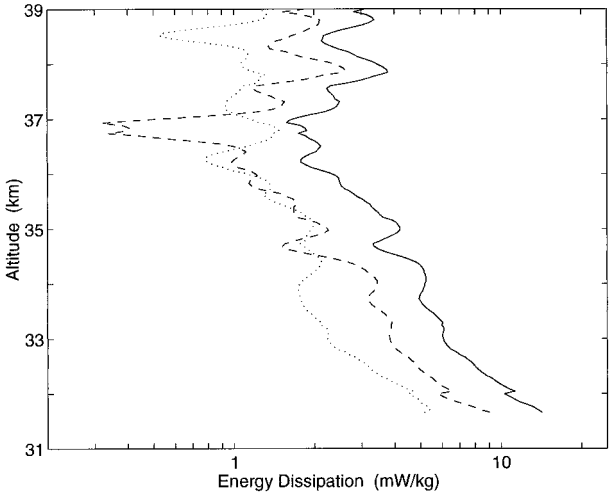

FIG. 2. Energy dissipation rates for the same integration limits as for Fig. 1.

the Purple Crow Lidar's Rayleigh-scatter system. The transmitter is a frequency-doubled Nd:YAG laser that outputs nominally 600 mJ per pulse at 20 Hz. The receiver is a 2.65-m diameter liquid mercury mirror. Details of the instrumentation are available in Sica et al. (1995).

3. Calculation of energy dissipation

Two basic methods for determining energy dissipation due to gravity waves are spectral methods and the tracking of individual gravity waves. Spectral methods use the temporal spectrum to estimate the energy dissipation. Knowledge of the wavenumber, power, and damping of an individual gravity wave also allows the energy dissipation to be calculated. As discussed by Hines (1965), the two methods allow for independent computations of the energy dissipation, as the energy dissipation for a single wave can be found independently of the gravity wave spectrum. We shall first calculate the energy dissipation using a spectral method and then use Prony's method to track an individual wave.

a. Spectral method

The temporal spectra in this study are computed using the covariance method of autoregressive (AR) modeling discussed in SR. The procedure used to determine energy dissipation is as follows. The temporal density perturbation spectra, which have units of seconds, first need to be converted to horizontal wind perturbations. Using the gravity wave polarization equations, the spectra are scaled by

$$\kappa = \left(\frac{g}{N}\right)^2 \tag{1}$$

(Gardner et al. 1989). Here g is the acceleration due to gravity and N is the angular buoyancy frequency, which is determined from the lidar's temperature measurements. The buoyancy frequency used in (1) is the background state N found from a polynomial fit to the buoyancy frequency measurements, though using either the mean or fitted N yields essentially the same final results. The wind spectral density obtained by multiplying the density perturbation power spectral densities (PSDs) by (1) has units of $(\text{m s}^{-1})^2$ s. The rms horizontal wind perturbation (in units of m s^{-1}) is found from the zeroth moment of the wind spectral density

$$U_{x_s} = \left(\int_{\omega_l}^{\omega_u} F_u(\omega)\, d\omega\right)^{1/2}, \tag{2}$$

where ω is the observed frequency, ω_l and ω_u the lower and upper limits of the integration, and

$$F_u(\omega) = \kappa(\text{PSD})_\omega \tag{3}$$

is the temporal power spectral density converted to a horizontal wind perturbation spectrum. The energy dissipation via the spectral method, ε_s, (in units of W kg^{-1}), is then the first moment of the horizontal wind perturbation spectrum,

$$\varepsilon_s = \int_{\omega_l}^{\omega_u} \omega\, F_u(\omega)\, d\omega. \tag{4}$$

The lower limit of the integration in (2) and (4) is the bandwidth of the measurement period. The upper limit is taken at the highest frequency possible before noise dominates the spectrum. The upper limit will be discussed in detail in the following section.

The uncertainties associated with this method are both statistical and theoretical. The statistical errors are small because the noise floor of the measurements is known; thus, the limits of integration can be chosen to minimize the contribution of the instrument noise to the signal. The major uncertainty is the appropriateness of the gravity wave polarization equations, particularly at high frequencies. At this stage it is perhaps safest to treat these values as order of magnitude estimates.

b. Prony's method

Energy dissipation of an individual wave can also be estimated using Prony's method. The AR, moving average, and autoregressive-moving average models discussed in SR use white noise as the driving input for the modeled process. If the input driving sequence is assumed to be damped sinusoids instead of white noise, the appropriate method is a technique named after Prony (Marple 1987). Prony's method is similar to fitting a Fourier series to the measurements, with two important differences. The first difference is the sinusoids can grow or decay in the Prony model. The second difference, and a major advantage of Prony's method, is that the wavenumbers (frequencies) are estimated directly from the spatial (temporal) data series. In the Fourier series the choice of the number of terms in the series chooses the locations used to compute the Fourier coefficients. In Prony's method the frequencies are estimated directly from the measurements.

The Prony model equation for real input data is

$$x[n] = \sum_{k=1}^{p/2} 2A_k e^{\alpha_k(n-1)\tau} \cos(2\pi m_k(n-1)\tau + \theta_k), \quad (5)$$

where the A's are the wave amplitudes, the α's the growth rate (negative for damping, positive for growth), the m's the wavenumbers (for spatial data series; for temporal series the m's would be frequency), and the θ's the phases of the waves. When p is even the model consists of $p/2$ damped cosines, otherwise when p is odd there are $p/2$ damped cosines plus a damped exponential.

The Prony model parameters are calculated in the following manner [see Marple (1987) for details]. The data sequence is approximated by a series of complex exponentials. The exponentials and their coefficients are initially unknown. It can be shown that the solution for the exponentials and their coefficients is separable, and the exponentials can be found in a manner similar to the covariance method for AR modeling. The exponentials are related to the wave's frequency and growth rate. The exponentials are then used to find their respective coefficients, which are related to the amplitude of the wave and its phase. A model order of $2p$ is thus required to fit p waves to the measurements. The choice of model order is made by specifying a sufficient amount of waves to accurately reproduce the measurements.

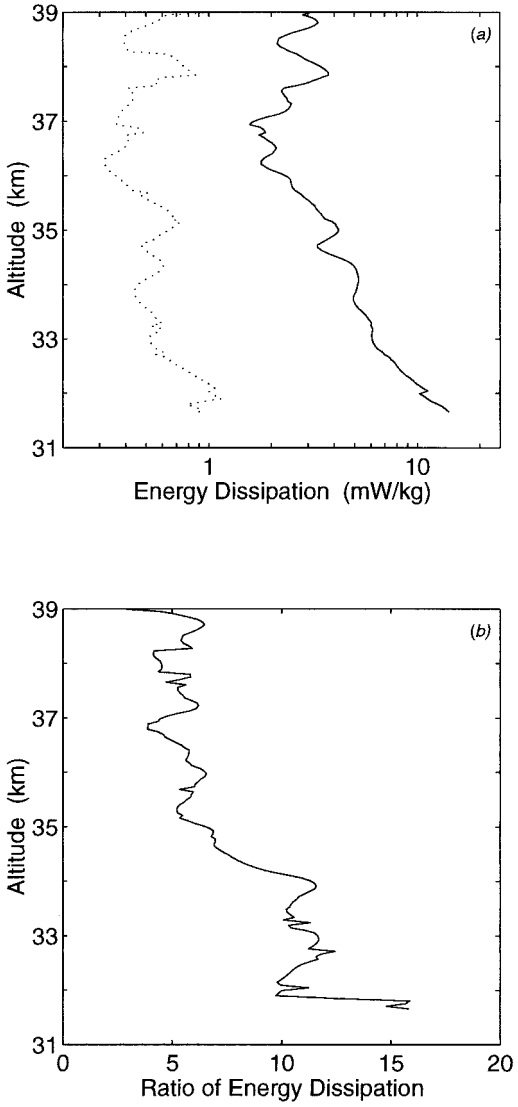

FIG. 3. Comparison of the energy dissipation rates calculated using the high-resolution temporal spectra with upper integration limits of the Nyquist frequency and 1 mHz. (a) Energy dissipation rates for the Nyquist integration (solid line) and the 1-mHz integration (dotted line). (b) The ratio of the two energy dissipation rate profiles.

An example of applying Prony's method to a spatial data series is shown in Fig. 4 of SR. This method was used by SR to decompose a test series to study the advantages and disadvantages of different spectral methods.

Energy dissipation via Prony's method can be found by fitting damped sinusoids to the vertical density perturbation measurements. Each spatial density perturbation data series is first fitted to a large number of waves, whose wavenumber, growth rate, amplitude, and phase are found. Once these wave parameters are computed, specific waves can be tracked as a function of time and the measured vertical phase velocity, which is assumed to be equal to the group velocity, v_g. The am-

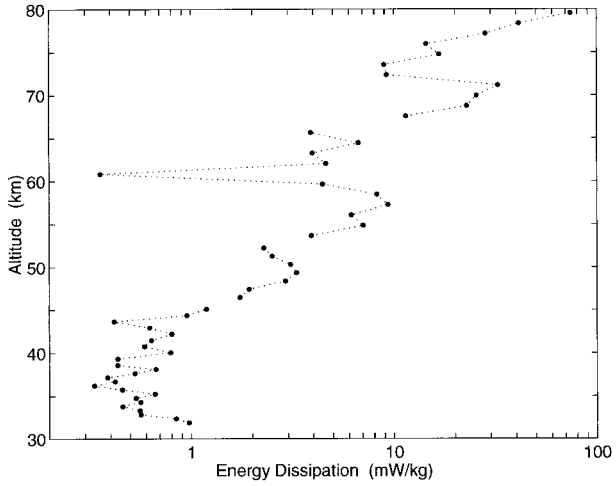

FIG. 4. Energy dissipation rate profiles for the stratosphere and mesosphere, using integrations out to 1 mHz, as described in the text.

plitude of the wave can then be expressed as an average horizontal wind fluctuation, U_x, using the polarization equations. The energy dissipation via Prony's method, ε_p, is then

$$\varepsilon_p = (\alpha v_g U_x^2)/2 \tag{6}$$

(Hines 1965). For Prony's method the horizontal wind perturbation due to a wave is found from the gravity wave polarization equations. The 90° phase shift between the density perturbations and horizontal wind perturbations needs to be taken into account when calculating ε_p as a function of height and time, as will be explained in the next section.

Like the spectral method, the errors in this method due to instrumental effects are straightforward to quantify. Prony's method fits individual waves to the data series, which summed together provide a best fit to the measurements. The number of waves is chosen to provide a fit that is significantly better than the noise floor of the measurements. The ''reality'' of a calculated wave can then be judged by its amplitude and growth rate relative to the amplitude and growth rate of the photon noise floor (which is known). For the case to be discussed below, a low wavenumber wave with large amplitude is chosen for study.

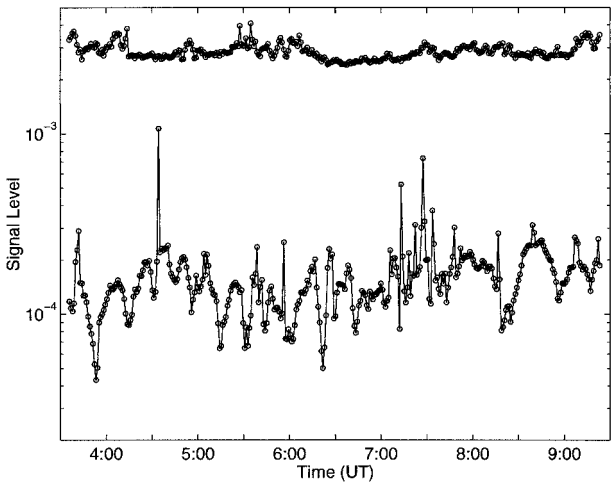

FIG. 5. Comparison of the photon noise floor of the measurements (upper curve) and the rms fit error for the Prony model (lower curve).

Such a wave has an amplitude well above the noise floor and has a wavenumber and frequency consistent with the assumptions of the gravity wave polarization equations. The most quantifiable error for Prony's method is in the choice of group velocity, which will be discussed in the next section.

4. Energy dissipation calculations

a. Spectral method

The temporal spectra in the upper stratosphere (31–39 km) have been discussed in SR and are shown in their Fig. 20. The strong peak at 2.1×10^{-3} s^{-1}, which is shown in Fig. 21 of SR, is strongest at heights below 35 km. The Nyquist frequency for these spectra is 8.2 mHz (for comparison the mean buoyancy frequency is 3.2 mHz). The rms wind fluctuation calculated using (2) is shown in Fig. 1 for three different integration limits. The solid line in Fig. 1 is the rms wind using an integration that begins at the bandwidth of the measurements [e.g., 1/(6 h)] and ends at the Nyquist frequency. The dotted line in Fig. 1 is the rms wind perturbations from the same lower limit out to the buoyancy frequency, whereas the dashed line shows the contribution to the rms wind by frequencies above the buoyancy frequency. The high-frequency region of the spectrum contributes about 20% of the rms wind variability.

The energy dissipation calculated by (4) is shown in Fig. 2 over the same three integration limits as in Fig. 1. The energy dissipation is highest below 35 km, as would be expected due to the strong features (and possible harmonics of this feature) above 2.1×10^{-3} s^{-1}. The increased contribution to the energy dissipation from the high frequencies is due to this feature as shown by the energy dissipation calculated from the buoyancy to the Nyquist frequency, which is larger than the energy dissipation calculated from frequencies lower than the buoyancy frequency below 35-km altitude. Above this altitude the feature disappears and the contributions of the two regions are more similar to each other.

Because the temporal spectra above 39 km have lower spatial–temporal resolution for comparable signal-to-noise ratios (as discussed in SR and shown in their Fig. 23), to calculate a comparable energy dissipation in the upper stratosphere and mesosphere the upper limit of the integration must be constrained to 1.0×10^{-3} s^{-1} for consistency. The effect of this cutoff on the energy dissipation calculated in the 31–39-km region is shown in Fig. 3. Decreasing the upper limit of the integration

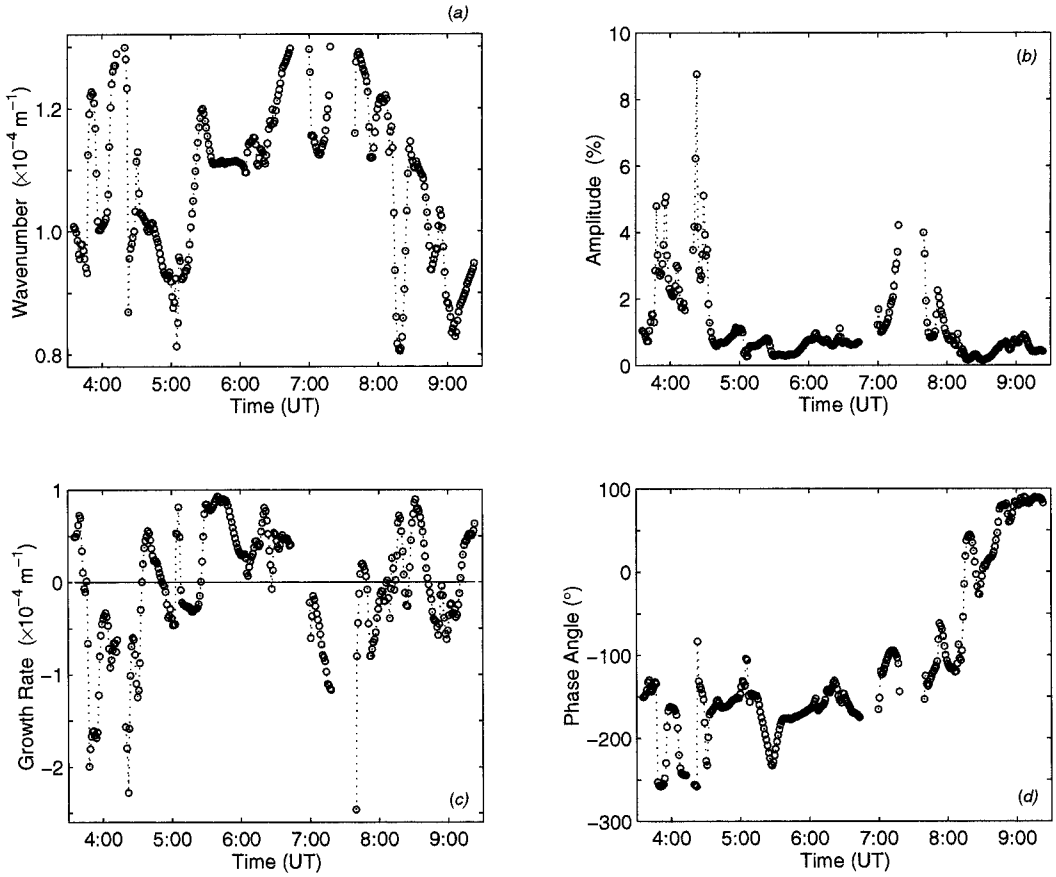

FIG. 6. Wave parameters deduced from Prony's method for the wavenumber band 1/(14 km) to 1/(7.7 km). (a) Time series of the retrieved wavenumber. (b) Time series of the wave amplitude. (c) Time series of the growth rate. A negative growth rate corresponds to a damped wave. (d) Time series of the wave's phase.

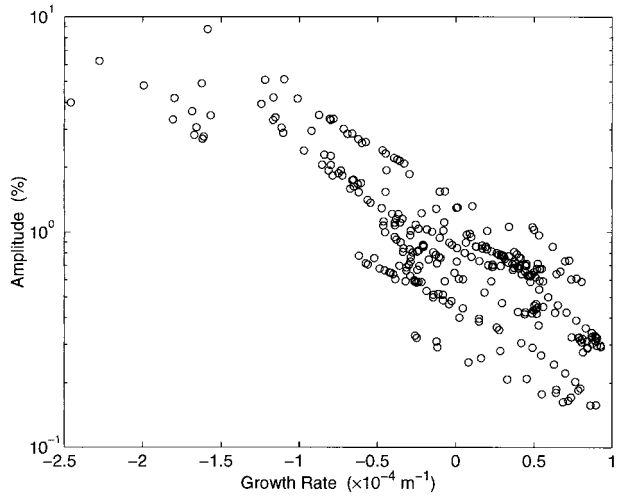

FIG. 7. Amplitude versus growth rate for the wave band shown in Fig. 6. The smallest amplitude waves have the largest growth rate, and the largest amplitude waves are the most heavily damped. At growth rates of less than -1×10^{-4} m^{-1} the wave amplitudes appear to saturate.

decreases the energy dissipation rate by about a factor of 8. This decrease should be kept in mind when comparing the energy dissipation rates at greater heights (Fig. 4). These calculations are likely lower limits to the energy dissipation. Figure 4 shows the energy dissipation between 31 and 80 km using the individual spectrum from the averages shown in Fig. 23 of SR. In general the energy dissipation increases above the stratopause except for a pronounced decrease in the energy dissipation around 60 km where the power in the spectrum dropped substantially over about 5 km in altitude.

b. Prony's method

In Prony's method the data series is represented in terms of decaying sinusoids using the L'_{sp} series from SR. For this series, the measurements are coadded to 144-m bins and 61-s temporal records, then temporally smoothed by a 21-point Kaiser–Bessel filter with a 21-min bandwidth. The Prony coefficients are calculated for 28 waves (i.e., an order of 56). This choice of order gave residuals to the fit about 20 times smaller than the photon noise floor of the measurements (Fig. 5).

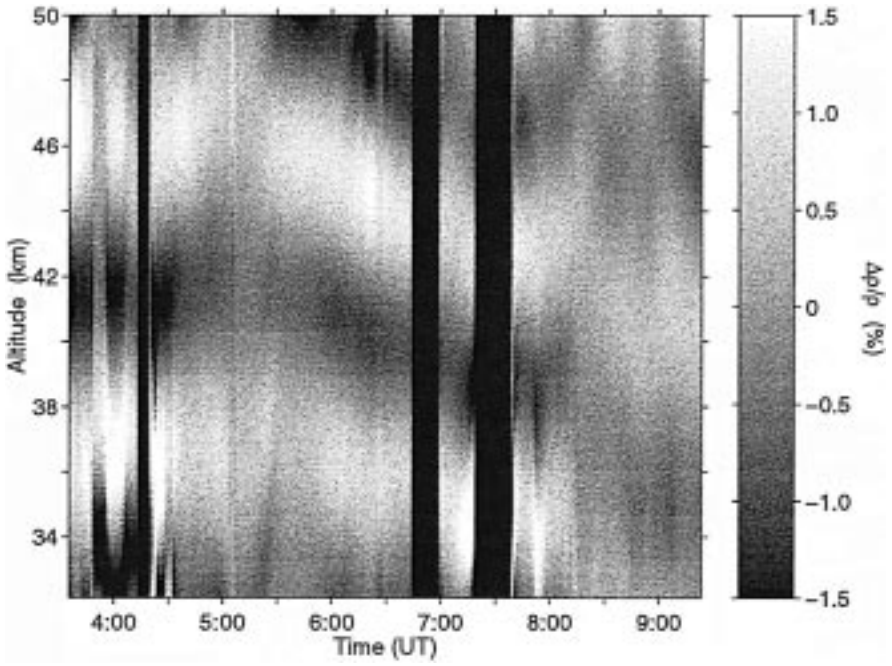

FIG. 8. The combination of the parameters shown in Fig. 6 allows a time–height contour of the density fluctuations in the low wavenumber band to be calculated. Dark vertical bands indicate times when the Prony method did not find a wave in the nominal 1/(10 km) vertical wavenumber passband. A color version of this figure can be found at http://PCL.physics.uwo.ca.

Once the parameters for the 28 waves were calculated for each of the 340 spatial data series, individual waves can be studied as a function of time. One waveband that had a clear feature was between 7.08×10^{-5} m^{-1} [1/(14.1 km)] and 1.25×10^{-4} m^{-1} [1/(8.0 km)]. Figure 6 shows the variability of the wavenumber, amplitude, growth factor, and phase in this wavenumber range. In the first hour the wavenumber is highly variable, whereas the amplitude is generally high and the growth factor initially positive (growth), then negative (damping). During this negative growth rate the wave(s) in this band are rapidly damped. The phase of the wave shows an overall increase after 0537 UTC until around 0900 UTC.

The amplitude of the wave(s) in this band can be plotted as a function of growth rate (Fig. 7). The points appear to lie in two distinct lines above and below a growth rate of -1×10^{-4} m^{-1}. Waves with little damping or waves that are growing in this passband have amplitudes that decrease with increasing growth rate in a roughly exponential manner. As the damping becomes on the order of twice the scale height (-7.1×10^{-4} m^{-1}) or greater the waves appear to saturate with amplitudes about 4%. Hence, the wave or waves appear to satisfy the basic growth rates and saturation of amplitude expected for gravity waves.

Using (5) the wave parameters in the low wavenumber band can be combined to form a height–time contour of the density perturbation (Fig. 8). Before 0537 UTC, there are no clear wave fronts and it is not clear if a single wave is present, or if a wave (or waves) could have formed and dissipated. However, from 0537 to 0923 UTC a clear wave exists with descending phase fronts. The amplitude of this wave varies between 0.5% and 2.0%.

To calculate the energy dissipation due to this wave, (6) requires the group velocity of the wave, in addition to the growth rate and amplitude (which is expressed as a horizontal wind fluctuation). Two periods were identified where the phase is monotonically increasing, 0537–0824 UTC and 0824–0923 UTC (Fig. 6d). The group (phase) velocity, determined by a linear least squares fit to the phase, which gives speeds of 0.22 ± 0.02 m s^{-1} and 0.87 ± 0.11 m s^{-1}, respectively, at these times. These errors include both the slope error from the regression line fitted to the phases and the relative deviation of the wavenumber over the period of interest (i.e., the wavenumber is not constant with time). The mean wavenumber is used to convert the time rate of phase change (in rad s^{-1}) into phase velocity (in m s^{-1}). From (6) the energy dissipation can then be determined, which has the same percent error as the group velocities (i.e., 7.6% between 0537 and 0824 UTC and 12.5% afterward).

A contour of the energy dissipation shows the substantial variations in space and time (Fig. 9). The mean energy dissipation is 0.15 ± 2.90 mW kg^{-1}, with only 37 of the 26 418 measurements (0.14%) having values greater than 15 mW kg^{-1} (all in the eastward phase of the velocity perturbation). Eighteen determinations of the energy dissipation were greater than 50 mW kg^{-1};

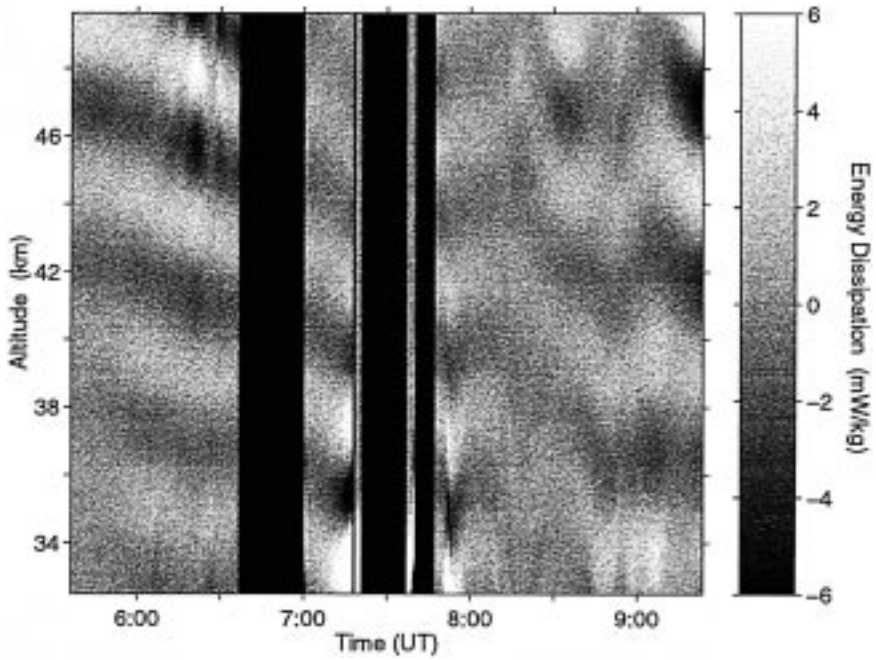

FIG. 9. Energy dissipation of the wave in the nominal 1/(10 km) vertical wavenumber band. Negative energy dissipation means the phase of the horizontal wind perturbation is westward. A color version of this figure can be found at http://PCL.physics.uwo.ca.

10 of these were in the range of 95 and 175 mW kg^{-1}. There is a large burst in energy dissipation around 0730 UTC at the lowest altitudes. This feature is clearly evident in the high-resolution vertical wavenumber spectra shown in SR (Fig. 10).

c. Comparison of the spectral and Prony energy dissipation calculations

The spectral and Prony energy dissipation calculations cannot be directly compared for several reasons. The Prony energy dissipation is calculated for a single wave with a mean wavenumber of 1.06×10^{-4} m^{-1} and a corresponding bandwidth of 1.35×10^{-5} m^{-1} (to the 3-dB points; the spectral bandwidth is equal to the mean growth rate divided by π). Hence, to compare the energy dissipation calculated by the two methods the spectral method energy dissipation must be calculated over the corresponding frequency range and bandwidth. Because the group velocity is known the corresponding frequency can be found to be 4.11×10^{-4} s^{-1}. Table 1 shows the values of the energy dissipation by the spectral method over a bandwidth corresponding to the 40-dB points.

To compare the Prony values to these calculations requires two factors to be considered. The first consideration is that energy dissipation via (6) uses peak amplitudes, whereas the spectral method uses rms amplitudes (Manson and Meek 1980). The second consideration is the time extent of the data series. The temporal spectra are obtained over 6 h and the Prony determinations are over a roughly 2-h period. The Prony determinations of energy dissipation–corrected rms values over a 6-h period are shown in the second line of Table 1. Above 39 km, the spectral determinations are about a factor of 2 smaller than the Prony determinations. However, below 39 km (where the Prony calculations and AR spectra showed the large power events) the Prony determinations are about 10 times larger than the spectral energy dissipation determinations.

A more ''stable'' subperiod of the Prony calculations is the 0537–0637 UTC period. Below 46 km the spectral determinations are now within a factor of 2 or better of the Prony determinations of energy dissipation. From 46 to 50 km they are approximately equal. Thus, it appears that the calculations via both methods are consistent with one another, with the spectral method calculation energy dissipation rates a factor of 2 smaller than the Prony's method for an individual wave.

5. Calculation of the eddy diffusion coefficient including saturation of the vertical wavenumber spectrum

The energy dissipation can be used to estimate the eddy diffusion coefficient. The eddy diffusion coefficient, D, is proportional to the energy dissipation and inversely proportional to the square of the angular buoyancy frequency:

$$D = \beta \frac{\varepsilon}{N^2}, \tag{7}$$

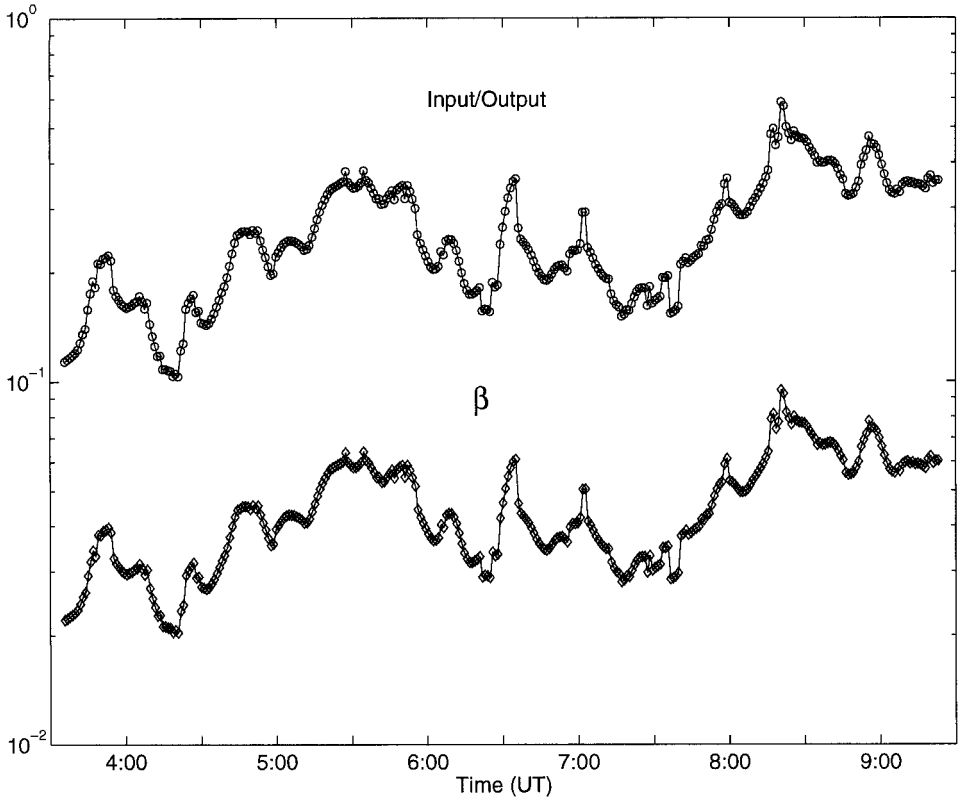

FIG. 10. The input–output ratio determined from the input driving noise of the autoregressive model and the total power of the output spectrum for the high spatial–temporal resolution vertical wavenumber spectrum. The spectrum is saturated at values of this ratio greater than unity, in the sense that the input driving noise variance of the process is then greater than the output power. The vertical axis on the rhs of the figure shows the corresponding β value used to compute the eddy diffusion coefficient, described in the text.

where β is traditionally taken as a constant. Hocking (1991) discusses the choices of β typically employed, with values in the range of 0.2 and 1.0 most common. However, it has recently been pointed out by McIntyre (1989) that β actually varies as a function of the saturation of the vertical wavenumber spectrum, expressed in his paper as the quantity $(a - 1)$. McIntyre gives a sample calculation of how the constant β varies with the saturation of the spectrum. The question is how can the amount of saturation of the spectrum be determined?

The parametric models independently estimate the driving noise variance of the input process (see SR for details). Hence, it seems reasonable that the amount of saturation, or gain, of the spectrum relates to the ratio of the ''input'' driving noise variance to the total ''output'' power (the area under the PSD). When the driving noise is less than the total power the spectrum is not saturated. When the driving noise exceeds the total power the output is saturated with respect to the input.

An example of this input–output ratio is shown in Fig. 10 for the same data series used for the Prony energy dissipation calculations with the input driving noise and total power computed by the covariance method (as discussed in SR). The vertical wavenumber spectra in the upper stratosphere on this night are all below the saturation line (i.e., there is gain in the system), with an average value of 0.26. At times, however, the ratio is greater than 0.5. The input–output ratio can be con-

TABLE 1. Comparison of the mean energy dissipation (mW kg^{-1}) calculated by the spectral method and Prony's method in different height ranges in the stratosphere. The spectral method is centered at 4.11×10^{-4} s^{-1} with a 40-dB bandwidth of 2.02×10^{-5} s^{-1}. The rms mean energy dissipation found by Prony's method is scaled to the 6-h extent of the spectral energy dissipation calculation.

Method	31–39 km	39–46 km	46–50 km	31–50 km
Spectral	2.44×10^{-2}	7.34×10^{-2}	1.61×10^{-1}	7.12×10^{-2}
Prony (0537–0923 UTC)	2.09×10^{-1}	1.50×10^{-1}	2.04×10^{-1}	1.89×10^{-1}
Prony (0537–0637 UTC)	5.13×10^{-2}	9.55×10^{-2}	1.63×10^{-1}	9.29×10^{-2}

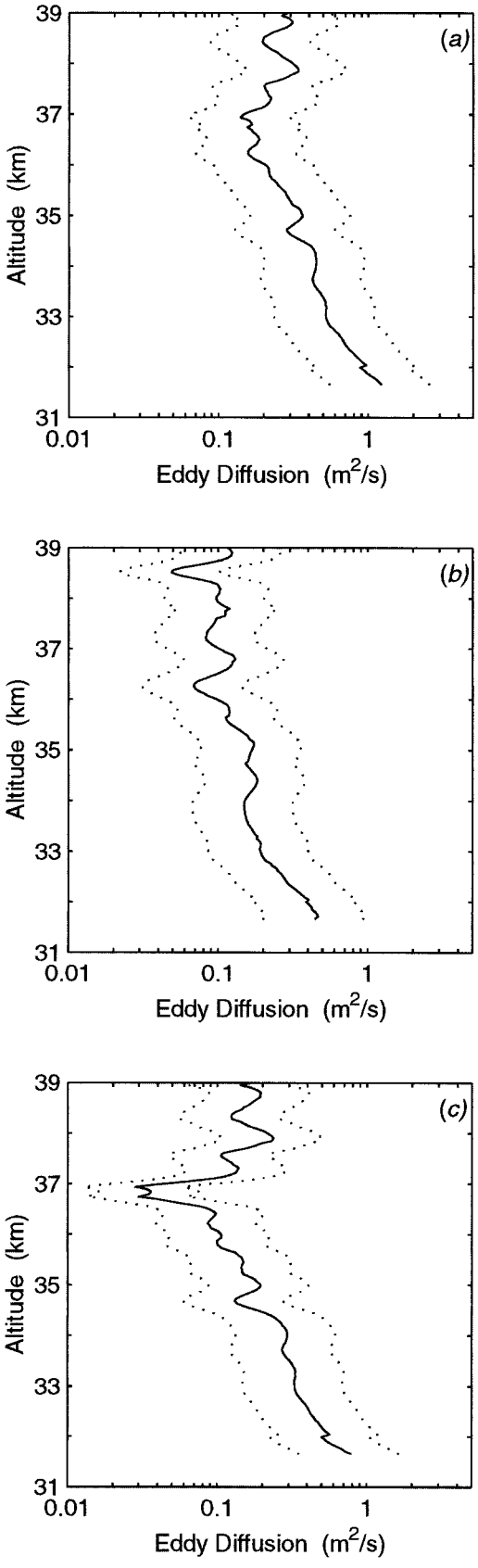

sidered an experimental determination of McIntyre's ($a - 1$) quantity; his Table 1 then relates this quantity to the β constant in the eddy diffusion coefficient equation. For this case, the mean value of β determined from McIntyre's Table 1 is 0.074, with a standard deviation of about 33%. This value of β is between a factor of 5–10 smaller than what has typically been assumed for the calculation of the eddy diffusion coefficient. In fact, it appears that the variations in the spatial spectrum, and their associated effect on β, is the largest source of uncertainty in the determination of the eddy diffusion coefficient.

6. Results of the eddy diffusion coefficient calculations

Eddy diffusion coefficient profiles in the stratosphere

Using the mean value of β calculated above and the measured mean-state buoyancy frequency, the eddy diffusion coefficient profile can be computed (Fig. 11). Three cases are shown based on the energy dissipation profiles shown in Fig. 2. Because β and N^2 are the same for each case, a similar situation exists as in Fig. 2; that is, below 35 km the features above the buoyancy frequency contributed about twice as much to the eddy diffusion value as the features below the buoyancy frequency, whereas above 35 km the contributions from below and above the buoyancy frequency are about the same. The magnitude of the eddy diffusion coefficients is between 0.1 and 1 $m^2\ s^{-1}$.

The eddy diffusion due to the wave highlighted in the Prony calculations is shown in Fig. 12. The eddy diffusion is large over a broad region relative to the minima. The mean rms eddy diffusion for this wave, scaled in time in a manner similar to the energy dissipation, is 0.021 $m^2\ s^{-1}$. This value is an order of magnitude or more less than the total eddy diffusion found by the spectral method. This result highlights the role of the highest frequency waves in providing most of the mixing. On the other hand, the β used for the Prony calculation is the same for the spectral calculation. Though the entire spectrum may be below saturation (as discussed above), in this low wavenumber band the spectrum may be closer to (or above) saturation, causing the eddy diffusion due to this wave to be underestimated.

Extending the calculation to the mesosphere requires using the lower spatial–temporal resolution spectra as

←

FIG. 11. The eddy diffusion coefficient for the high spatial–temporal resolution case using the β value shown in Fig. 10. The dotted lines show the mean deviation of the eddy diffusion coefficient due to the variations of β (i.e., $\sigma_\beta/\beta = 33\%$ for this case). (a) Using the integration limits from the sampling frequency to the Nyquist frequency as in Fig. 1. (b) Using the integration limits from the sampling frequency to the buoyancy frequency. (c) Using the integration limits from the buoyancy frequency to the Nyquist frequency.

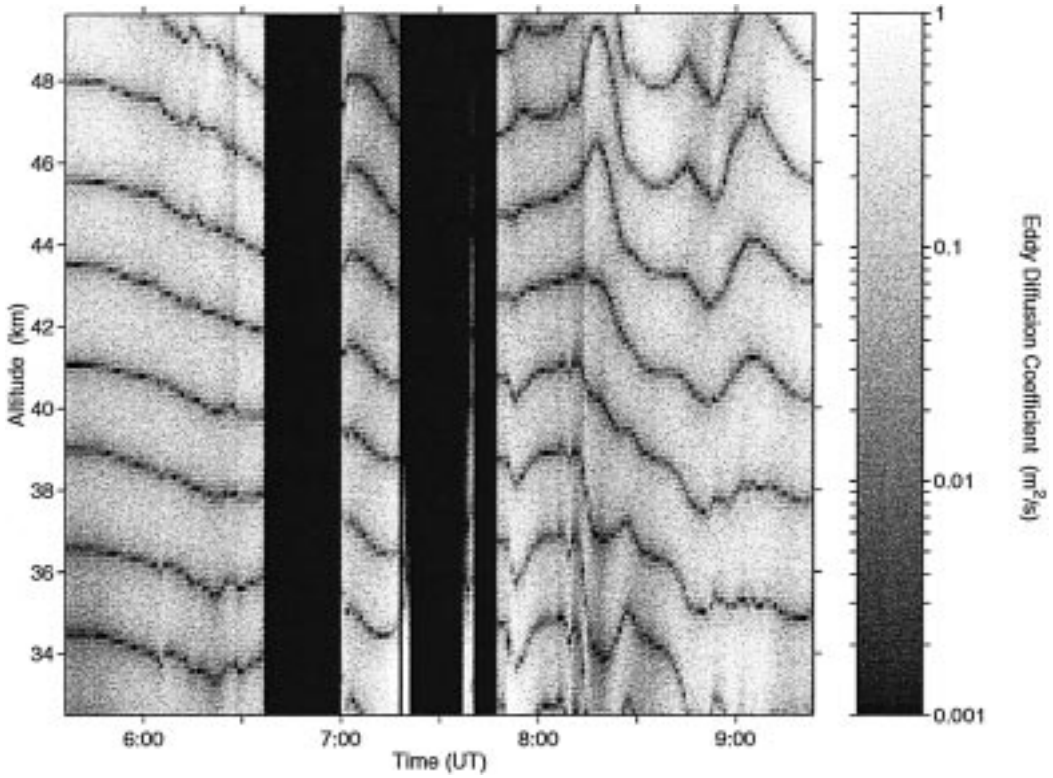

FIG. 12. Eddy diffusion coefficient derived from Prony's method for the nominal 1/(10 km) wavenumber wave shown on a logarithmic scale. Note the broad band of high dissipation relative to the narrow bands of low dissipation. A color version of this figure can be found at http://PCL.physics.uwo.ca.

in the calculation of energy dissipation. The effect of using 1×10^{-3} s^{-1} as the upper limit of the integration for the 31–39-km spectra is shown in Fig. 13. The eddy diffusion coefficient is underestimated by a factor of 15–20. The difference is larger than for the energy dissipation because the spectral cutoff also effects the calculation of β. As in the energy dissipation case, cutting off the intense high-frequency features at the lower altitude causes a larger underestimation of the eddy diffusion coefficient.

The major source of uncertainty in this calculation of the eddy diffusion coefficient may lie in the estimation β using the degree of vertical wavenumber spectrum saturation. In the high-resolution spatial case a value of 0.044 is used for β; the corresponding average values of β using the L_{sp}, M_{sp}, and H_{sp} data series from SR are shown in Table 2. As one would anticipate, the spectrum is more saturated at greater height as is reflected by the larger values of β above the stratopause. Figure 14 shows the time variation of the input–output ratios and the corresponding β's. Note the spectrum is nearly saturated in the lower mesosphere (and indeed saturated around 0800 UTC) and is completely saturated until 0600 UTC in the upper mesosphere.

The resulting eddy diffusion coefficient profile in the stratosphere and mesosphere using the β values discussed above is shown in Fig. 15. The time variation of β is indicated by the horizontal bars. The small energy dissipation in the 60-km height region is evident by the smaller eddy diffusion coefficient at these heights. The eddy diffusion coefficient varies from about 0.01 to 70 m^2 s^{-1} from 30 to 80 km.

7. Discussion

The energy dissipation calculated by two independent methods, a spectral method and a method that tracks individual waves using Prony's method, is consistent and gives some confidence in the methodology of the study. In Prony's method the frequency, amplitude, damping, and phase of individual waves are estimated from the density fluctuation measurements. The ability to investigate individual wave structures in a ''saturated'' spectrum using Prony's method appears to be a useful application of this technique.

An estimate of the eddy diffusion coefficient profile is made, attempting to account for the dependence of the constant in (7) on the degree of vertical wavenumber spectral saturation, as suggested by McIntyre (1989). This technique appears promising since spectral saturation can now be estimated from the measurements using an autoregressive parametric model of the spectrum to measure the ratio of the input to output power (gain). The eddy diffusion profiles obtained seem rea-

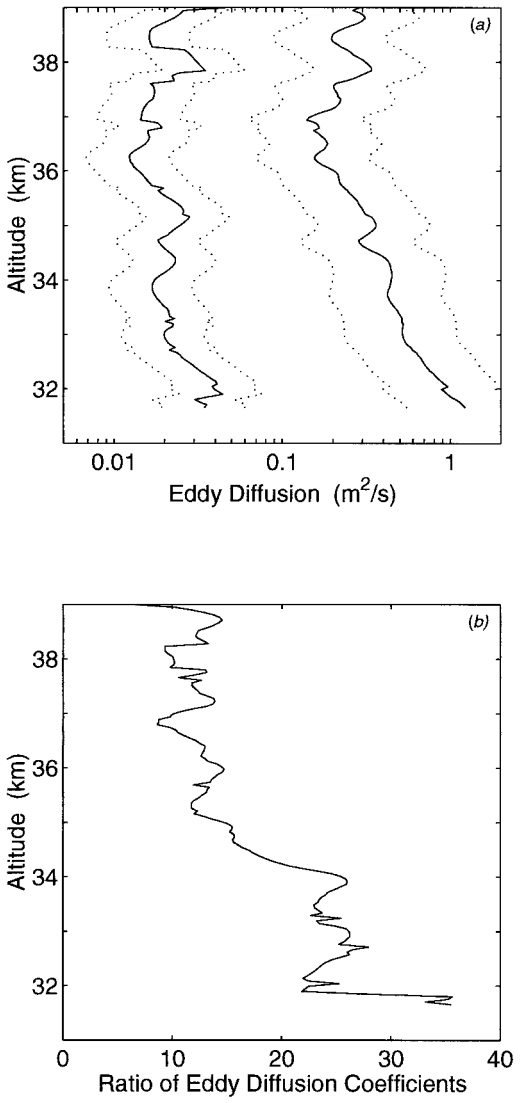

FIG. 13. Comparison of eddy diffusion coefficient profiles for two different integration limits. (a) Both curves have lower integration limits of the sampling frequency and upper integration limits of the Nyquist frequency (solid line) and 1 MHz (dotted line) similar to Fig. 3. (b) Ratio of the two curves. The larger ratio than in the energy dissipation case is due to the differences in β values retrieved from the lower- and higher-resolution vertical data series, in addition to the differences in energy dissipation using different integration limits.

sonable when compared to other estimates. Hocking (1991) has assembled a large body of eddy diffusion coefficient estimates from the ground to the turbopause. In the upper stratosphere the 1 standard deviation range of the eddy diffusion coefficients ranges from about 0.3 to 20 $m^2 s^{-1}$, whereas in the mesosphere the values range from about 3 to 300 $m^2 s^{-1}$. Assuming a nominal β value of 0.5 and a buoyancy frequency of 1/(5 min) these eddy diffusion coefficients correspond to energy dissipation rates of between 1 mW kg^{-1} and 70 mW kg^{-1} in the stratosphere and between 10 mW kg^{-1} and 1000 mW kg^{-1} in the mesosphere. Both the height variation of this ensemble of measurements and the magnitudes compare favorably with the eddy diffusion coefficients calculated from the lidar measurements, though the magnitude of the particular eddy diffusion profile calculated for this night is a bit smaller than the 1 standard deviation range shown by Hocking for the full-height range case. Increasing the full-height range eddy diffusion profile by a factor of 15–20 suggested by the comparison to the high-resolution case (Fig. 13) would put the estimate in Hocking's range of previous measurements.

TABLE 2. Ratio of the input driving noise to the average power for the three height regions used for the average temporal spectrum in the upper stratosphere and mesosphere and the corresponding value of β from McIntyre (1989).

Height range (km)	Mean input–ouput ratio	β
32–50	0.102	0.020
50–65	0.497	0.079
65–80	2.53	0.344

However, it must be emphasized that the eddy diffusion coefficient estimates presented in this study attempt to account for the degree of spectral saturation. The eddy diffusion coefficients presented in the Hocking (1991) review presumably use β values on the order of 0.5, that is, about 10 times larger than the β derived from the input–output ratio for the high resolution case in the stratosphere. Because the eddy diffusion coefficients are of the correct magnitude, this result suggests that the calculated energy dissipation by both the spectral method and Prony's method are fairly large. Medium frequency (MF) radar estimates of the energy dissipation in the upper mesosphere typically obtain values for the energy dissipation of about 0.1 mW kg^{-1} (e.g., Manson and Meek 1980), although a recent reevaluation of the calculation of these rates from measured spectral widths by MF radar shows these values may be a factor of 2–3 high (Hocking 1996). The energy dissipation rate is also highly variable in height and season. For instance, Lübken et al. (1993) measured rates of 1–2 mW kg^{-1} in the high-latitude winter mesosphere. Similar instrumentation has been flown at midlatitudes and obtained much higher values of energy dissipation (W. Hocking 1997, personal communication). Hence, the energy dissipation rates derived from the lidar measurements seem to be reasonable.

The relatively high values of energy dissipation obtained in this study may simply be due to an overestimation of the horizontal wind fluctuations from the gravity wave polarization equations. However, there is evidence to suggest the differences may be real. The Rayleigh-scatter lidar temperature profiles have been used to deduce regions of stability and instability in the upper stratosphere and mesosphere via measurements of the lapse rate (Sica and Thorsely 1996). It is becoming apparent that on many nights the geophysical var-

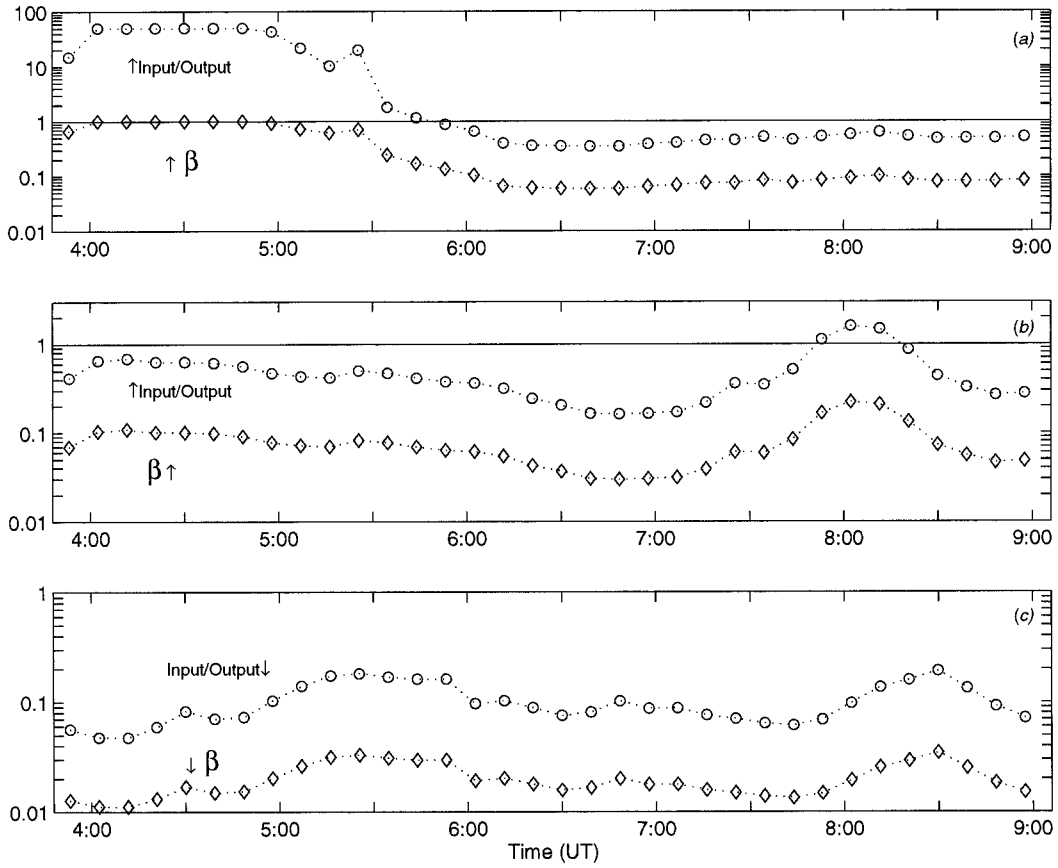

FIG. 14. The input–output ratio and β for the low-resolution case for altitude regimes (a) 60–80 km, (b) 45–65 km, and (c) 32–50 km. Above the ''saturation line'' the input driving noise is greater than the output power in the spectrum. The β value is at its maximum possible value during the 0425–0449 UTC period in the 60–80-km region, as the total power in the spectra during this period times was very small (i.e., an input–output ratio > 50).

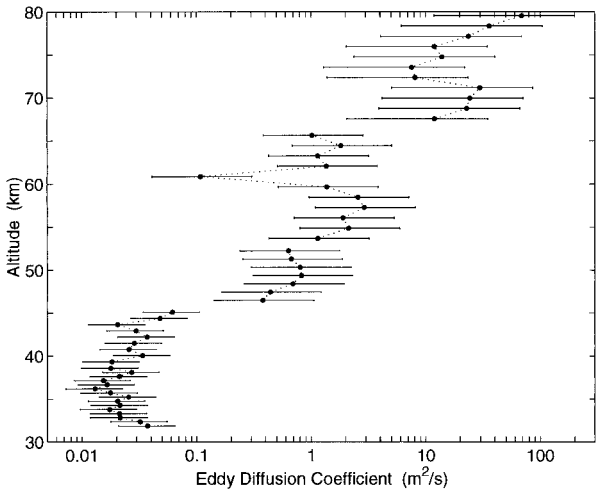

FIG. 15. Eddy diffusion coefficient profile for the stratosphere and mesosphere. The points use the mean β from the high-resolution case. The horizontal bars give a measure of the variability of the β value.

iations are of sufficient magnitude that isolated regions of superadiabatic lapse rate exist throughout the middle atmosphere. The amount, duration, and intensity of these events, particularly in the upper stratosphere, may in part explain why the energy dissipation is large on this particular night. These measurements will be tested in the future by comparison of the energy dissipation derived from measurements with the University of Western Ontario's MF radar and the sodium resonance–fluorescence lidar, which will allow high temporal–spatial measurements of temperature profiles to be made in the upper mesosphere and lower thermosphere.

If the degree of spectral saturation is truly related to the input–output power ratio, then the β value for the eddy diffusion coefficient should be related to the average power in the spectrum. In SR, the use of the Hines wavenumber in characterizing the nonlinear tail region of the vertical wavenumber spectrum is discussed. A relation between these parameters may be anticipated and does indeed exist (Fig. 16). As the Hines wavenumber increases so does the value of β, as is clear for all the available data series. The rate of increase of β is greater at higher altitudes.

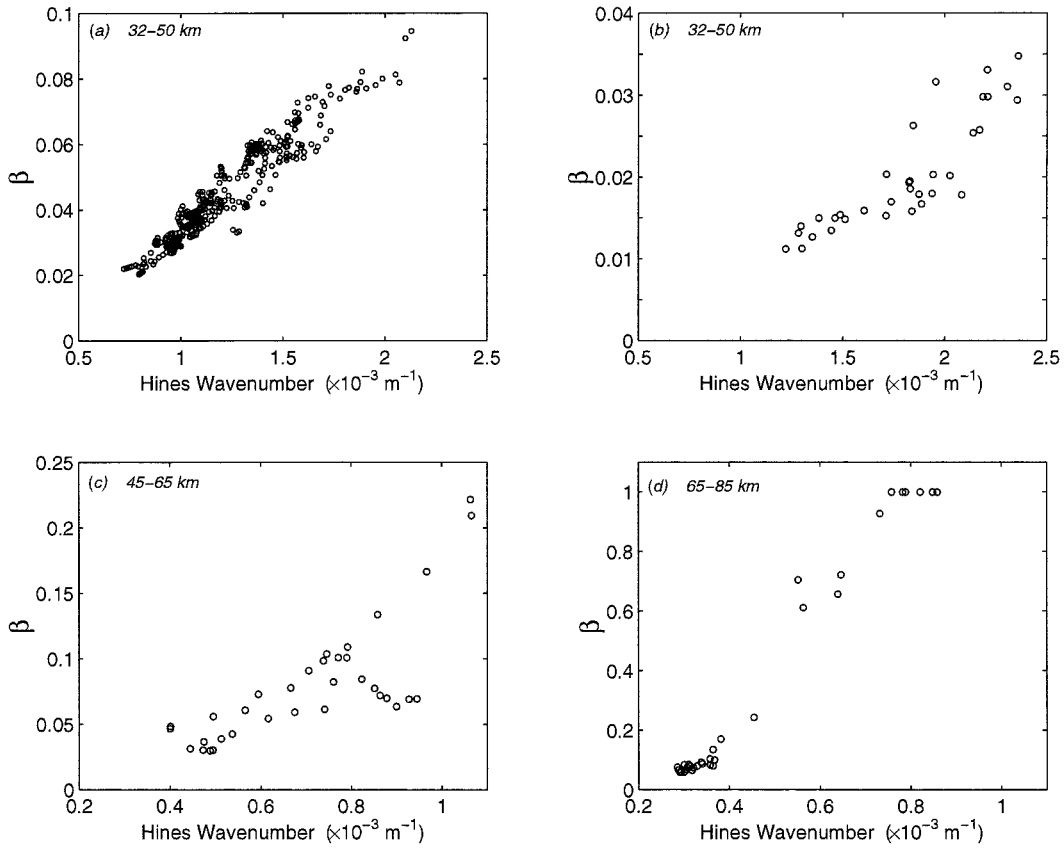

FIG. 16. The increase of the constant β with increasing Hines wavenumber. (a) High-resolution data series in the stratosphere. (b)–(d) In the three height ranges from Table 1, 32–50 km, 50–65 km, and 65–80 km, respectively. For a given vertical bandwidth β increases with increasing Hines wavenumber. Increasing Hines wavenumber means more of the tail spectrum is linear. The Hines wavenumber decreases with increasing height. The value of β increases with height for a given value of the Hines wavenumber, in addition to increasing more rapidly with Hines wavenumber at the greatest heights.

Physically, this result means that as the tail spectrum becomes more linear (i.e., the Hines wavenumber increases) the input–output ratio begins to saturate and there is no gain in the system; the atmospheric wave ''amplifier'' becomes less efficient. As the tail becomes more nonlinear, the average power is higher, and the additional energy appears at low wavenumbers, steepening the slope of the spectrum. As the vertical wavenumber spectrum evolves temporally (as shown in SR), the low wavenumber part of the spectrum increases and then decreases in intensity. During the time of increasing power the tail spectrum is mostly nonlinear and the atmosphere wave amplifier is highly efficient (i.e., the gain is large). As the average power decreases, perhaps due either to changes in the source region(s) or the background winds (or both), the energy dissipation increases as the tail spectrum becomes more linear. The amplifier is now more inefficient (i.e., lower gain), and more of the input power is being diverted to the generation of smaller scale size eddies rather than wave growth. This result is contrary to our initial expectation of eddy diffusion increasing as the tail spectrum becomes more nonlinear.

8. Conclusions and future directions

Parametric models have proven a powerful tool for the analysis of the high spatial–temporal measurements now available from the Purple Crow Rayleigh-scatter lidar. A detailed analysis of energy dissipation and eddy diffusion using a night's measurements leads us to the following conclusions.

1) Energy dissipation can be estimated by two independent techniques. The spectral method estimates the energy dissipation from the horizontal wind velocity spectral density. Prony's method allows the attributes of a wave (or waves) in a prescribed wavenumber band to be determined and the energy dissipation to be calculated independently of the form of the spectrum. This calculation results in nominal values for the energy dissipation of 1 mW kg^{-1} and eddy diffusion coefficient of 0.3 $m^2 s^{-1}$ in the stratosphere.
2) The energy dissipation rate determined by the above techniques is consistent with previous determinations of the energy dissipation in the upper stratosphere and mesosphere.

3) A combination of the information obtained from the parametric models and the theoretical work of McIntyre (1989) has been used to deduce the value of β, the multiplicative constant necessary to compute eddy diffusion coefficients from energy dissipation rates. The constant, which can be related to the degree of vertical wavenumber spectral saturation, is determined to be a factor of 5–10 smaller than assumed in many previous studies.
4) The eddy diffusion coefficients derived from the measurements agree with previous measurements in both magnitude and height variation, using the revised β values.
5) The magnitude of β is proportional to the Hines parameter, the wavenumber in the tail spectrum above which nonlinear processes determine the spectral shape. Hence, it is speculated that the increases in β are associated with an ''unloading'' of the gravity wave tail spectrum into turbulence as the vertical wavenumber spectral energy decreases and a ''filling'' of the spectrum as β decreases. These vertical wavenumber spectrum changes for decreasing β are particularly noticeable at low wavenumbers as the tail becomes more nonlinear, the average power greater, and a decreased amount of turbulence is generated.

Studies are under way to characterize the energy dissipation and the eddy diffusion as a function of season. Furthermore, Prony's method is being used to isolate individual wave events for comparison with MF radar and sodium lidar measurements in the manner described by Manson (1990).

Acknowledgments. I thank Professor M. McIntyre for his insights into the calculation of the eddy diffusion coefficient and Professors W. Hocking, C. Gardner, and T. Shepherd for valuable scientific discussions. Thanks also go to Team Purple Crow, in particular Dr. S. Argall, S. Beatty, Albert Russell, M. Thorsley, and David Kwarciak. This work was supported by grants from the National Scientific and Engineering Research Council, the Canadian Space Agency, CRESTech, and Canada's Atmospheric Environment Service.

REFERENCES

Blix, T. A., E. V. Thrane, and O. Andreassen, 1990: In situ measurements of the fine-scale structure and turbulence in the mesosphere and thermosphere by means of electrostatic positive ion probes. *J. Geophys. Res.,* **95,** 5533–5548.

Gardner, C. S., M. S. Miller, and C. H. Liu, 1989: Rayleigh lidar observations of gravity wave activity in the upper stratosphere at Urbana, Illinois. *J. Atmos. Sci.,* **46,** 1838–1854.

Hines, C. O., 1965: Dynamical heating of the upper atmosphere. *J. Geophys. Res.,* **70,** 177–183.

Hocking, W. K., 1991: The effects of middle atmosphere turbulence on coupling between atmospheric regions. *J. Geomagn. Geoelectr.,* **43** (Suppl.), 621–636.

——, 1996: An assessment of the capabilities and limitations of radars in measurements of upper atmosphere turbulence. *Adv. Space Res.,* **17,** 37–48.

Lübken, F.-J., W. Hillert, G. Lehmacher, and U. von Zahn, 1993: Experiments revealing small impact of turbulence on the energy budget of the mesosphere and lower thermosphere. *J. Geophys. Res.,* **98,** 20 369–20 384.

Manson, A. H., 1990: Gravity wave horizontal and vertical wavelengths: An update of measurements in the mesopause region (~80–100 km). *J. Atmos. Sci.,* **47,** 2765–2773.

——, and C. E. Meek, 1980: Gravity waves of short period (5–90 min), in the lower thermosphere at 52°N (Saskatoon, Canada). *J. Atmos. Terr. Sci.,* **42,** 103–113.

Marple, S. L., 1987: *Digital Spectral Analysis.* Prentice-Hall, 492 pp.

McIntyre, M. E., 1989: On dynamics and transport near the polar mesopause in summer. *J. Geophys. Res.,* **94,** 14 617–14 628.

Sica, R. J., and A. T. Russell, 1999: Measurements of the effects of gravity waves in the middle atmosphere using parametric models of density fluctuations. Part I: Spatial and temporal spectra. *J. Atmos. Sci.,* **56,** 1308–1329.

——, and M. D. Thorsley, 1996: Measurements of superadiabatic lapse rates in the middle atmosphere. *Geophys. Res. Lett.,* **23,** 2797–2800.

——, S. Sargoytchev, P. S. Argall, E. F. Borra, L. Girard, C. T. Sparrow, and S. Flatt, 1995: Lidar measurements taken with a large-aperture liquid mirror. Part 1: Rayleigh-scatter system. *Appl. Opt.,* **34,** 6925–6936.